Available online at www.CivileJournal.org

Civil Engineering Journal

(E-ISSN: 2476-3055; ISSN: 2676-6957)

Vol. 12, No. 05, May, 2026

Anchorage Performance of Headed Reinforcement Bar Embedded in Roof Exterior Beam-Column Joints

Zev Al Jauhari [1*], Tomoya Matsui [1]

[1] *Department of Architecture and Civil Engineering, Toyohashi University of Technology, Toyohashi 441-8580, Japan.*

Received 05 February 2026; Revised 19 April 2026; Accepted 23 April 2026; Published 01 May 2026

Abstract

The anchorage behavior of headed reinforcement bars embedded in roof exterior beam–column joints is influenced by the presence and configuration of supplementary reinforcement bars. This study aims to develop an improved predictive formulation for anchorage capacity by introducing a modification factor that accounts for the effect of supplementary bars through a combined numerical and analytical approach. A three-dimensional nonlinear FE model was developed and validated against previously reported pullout test results for load–displacement response, crack propagation, reinforcement strain behavior, and stress distribution. The numerical results showed agreement with experimental observations and accurately captured the failure modes. To further interpret the internal force mechanism, a three-dimensional strut-and-tie model (STM) was formulated based on principal stress trajectories obtained from FE analysis. The proposed STM successfully predicted the anchorage capacity, consistent with the experimental results. Parametric studies revealed that increasing the supplementary bar ratio significantly enhances pullout capacity by enlarging the compression strut area and improving confinement within the joint region. Based on regression analysis of the STM results, a new coefficient was introduced to refine the modified Kubota and Murakami empirical formula, incorporating the effect of supplementary bar ratio. The revised formulation provides improved prediction accuracy with low statistical dispersion.

Keywords: Headed Reinforcement Bar; Concrete Breakout Strength; Beam-Column Joint; Pullout Load, Finite Element Analysis; STM.

1. Introduction

Beam–column joints (BCJs) are critical regions in reinforced concrete (RC) structures, where horizontal and vertical structural elements intersect. The behavior of these joints largely governs the overall performance of the structure, as they must effectively transfer forces between beams and columns while maintaining the structural integrity of the entire framework. Generally, conventional anchorage methods using straight bars and hooks are employed in BCJs to achieve the required load-resisting capacity. In recent years, there has been growing interest in the use of headed reinforcement bars, or mechanical anchorages, as alternatives to conventional hooked bars, primarily to improve reinforcement detailing efficiency and ease of construction in these highly congested regions [1]. In RC members with headed reinforcement bars, transverse reinforcement is commonly placed near the bar head and along the bar length, as shown in Figure 1. Per ACI 352R-02 [2], based on a previous study [3], connection stirrups or hoop legs should be provided close to the head at the BCJ to prevent concrete side blowout. Because side blowout failure is governed by the tensile resistance of the concrete cover, the presence of transverse reinforcement is expected to enhance the tensile capacity and, consequently, the anchorage performance.

* Corresponding author: zev.al.jauhari.bf@tut.jp

https://doi.org/10.28991/CEJ-2026-012-05-02

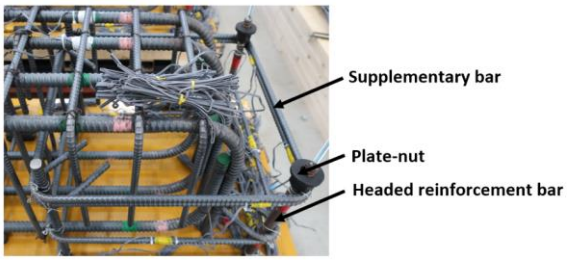

Figure 1. Headed reinforcement and transverse reinforcement bars in concrete member

The anchorage behavior of headed reinforcement bars is strongly influenced by the surrounding concrete and the presence of transverse or supplementary reinforcement. In particular, side blowout failure, which is governed by the tensile capacity of the concrete cover, is a critical concern in BCJs. Previous studies have investigated the role of transverse reinforcement in mitigating such failures. Several researchers reported that transverse reinforcement enhances anchorage capacity by confining the concrete and restraining crack propagation [4-6]. Conversely, other studies observed that while transverse reinforcement improves ductility and post-peak behavior, its influence on ultimate anchorage capacity may be limited [7]. These contrasting findings indicate that the effectiveness of transverse reinforcement depends on factors such as its configuration, orientation, and interaction with the surrounding concrete, and thus remains not fully understood.

Roof exterior BCJs represent a critical, less-confined structural condition, where reduced surrounding structural restraint makes them more vulnerable to anchorage failure, particularly concrete side blowout. Compared to interior joints, the stress distribution and confinement mechanism in roof exterior joints are significantly different, making them a conservative and critical case for evaluating anchorage performance. Several investigations have examined the anchorage performance of headed bars in concrete members. Nevertheless, experimental research on headed bars installed in roof exterior BCJs, particularly with supplementary hoop reinforcement, remains limited.

To overcome the limitations of experimental studies, numerical methods, such as three-dimensional finite element analysis (FEA), have been widely used to investigate anchorage behavior in RC structures [8]. FEA enables detailed evaluation of internal stress distribution, crack development, and load-transfer mechanisms that are difficult to capture experimentally. In addition, analytical approaches such as the strut-and-tie model (STM) provide a simplified yet rational framework for interpreting the mechanisms of force transfer in discontinuity regions of concrete structures. Previous studies have shown that STM can effectively represent the load transfer in members with headed reinforcement [9–12]. However, most existing applications have focused on deep beams, lap splices, or interior connections, and the application of STM to roof exterior BCJs, particularly considering the influence of supplementary reinforcement, remains insufficiently explored.

Recent advancements have significantly improved the understanding of the anchorage behavior of headed bars embedded in RC members by considering both geometric design and material-related effects through experimental tests, FE simulations, and theoretical analyses. Yuan et al. [13], through experimental and analytical investigations, demonstrated that headed bars used as shear reinforcement achieve more efficient and reliable anchorage via a bearing-dominated mechanism, in which appropriate head size and embedment allow full development of bar strength and improved performance compared to conventional hooked bars. Mirzagulpour et al. [14], based on pull-out tests of headed reinforcing bars embedded in alkali–silica reaction (ASR)-affected concrete, reported that ASR can enhance anchorage capacity due to confinement-induced self-prestressing, despite reducing concrete tensile strength and ductility. In addition, recent numerical studies have incorporated innovative materials and joint configurations, such as shape-memory-alloy reinforcement in BCJs, demonstrating enhanced structural response and resilience under loading [15]. Substantial progress has also been made in the analytical and numerical modeling of discontinuity regions (D-regions), where stress distributions are highly nonlinear. Comprehensive reviews have highlighted the importance of integrating FEA with rational idealizations such as the STM to accurately capture load-transfer mechanisms in RC structures [16]. Recent developments have further advanced this approach by incorporating lattice-based and hybrid modeling techniques, enabling a more refined representation of internal force flow and structural behavior [17]. Nevertheless, despite these advancements, the application of such integrated approaches to roof exterior BCJs, particularly considering the role of supplementary reinforcement in headed bar anchorage, remains limited.

Experimental investigations on headed reinforcement bars embedded in roof exterior BCJs have provided valuable insights into their anchorage mechanisms [18, 19]. These studies demonstrate that pullout resistance is governed by the interaction between diagonal compressive stresses in the concrete and tensile forces carried by supplementary reinforcement, as shown in Figure 2. However, the available experimental data are limited in scope, particularly for variations in supplementary reinforcement parameters such as diameter and quantity. This limitation restricts a comprehensive understanding of the anchorage behavior in such structural configurations.

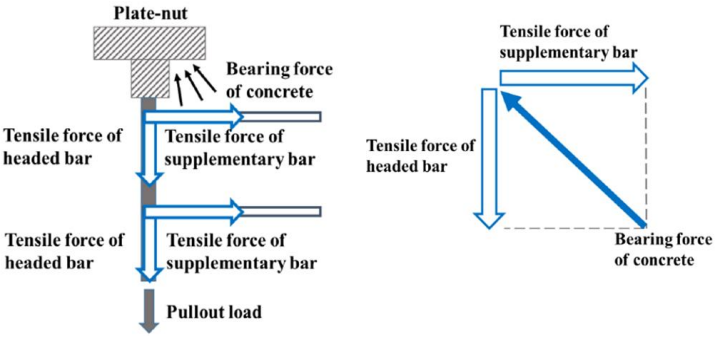

Figure 2. Force transfer mechanism of headed and transverse reinforcement bars in concrete member [18]

Furthermore, existing empirical models for predicting anchorage capacity, such as the modified Kubota and Murakami formulation [19, 20], provide reasonable estimations but do not explicitly account for the influence of supplementary reinforcement parameters. As a result, their applicability to configurations with varying supplementary reinforcement ratios is limited.

To address these gaps, this study investigates the anchorage performance of headed reinforcement bars embedded in roof exterior BCJs with a particular focus on the role of supplementary reinforcement. A 3-D nonlinear FE model is developed and validated against experimental results to accurately capture load–displacement behavior, crack propagation, and stress distribution. Based on the principal stress trajectories obtained from numerical analysis, a 3-D STM is formulated to represent the internal force transfer mechanism. Furthermore, a comprehensive parametric study is conducted to evaluate the influence of supplementary reinforcement diameter and quantity on anchorage capacity. Finally, a modified empirical formulation is proposed by introducing a new coefficient that accounts for the supplementary reinforcement ratio, thereby improving the predictive accuracy of existing design equations.

1.1. Theoretical Approach

The theoretical approach of this study is grounded in the mechanics of force transfer in reinforced concrete discontinuity regions, where anchorage behavior is governed by the interaction between bearing stresses, bond resistance, and concrete fracture. When a headed reinforcement bar is subjected to tensile loading, the applied force is transferred to the surrounding concrete through a combination of bearing at the head and bond along the embedded length, leading to the development of compression struts and tensile stress fields within the joint region. Failure typically occurs as a concrete cone breakout or a side blowout, depending on the confinement conditions and stress distribution. To capture these mechanisms, this study adopts a multi-level theoretical approach integrating nonlinear FEA and STM. The FEA is based on continuum mechanics and nonlinear constitutive relationships, enabling detailed representation of stress fields, crack initiation, and propagation within the concrete. In parallel, the STM is employed as a simplified yet theoretically rigorous representation of internal force flow, rooted in lower-bound plasticity theory, in which equilibrium is satisfied through an idealized truss analogy of compression struts and tension ties. The principal stress trajectories obtained from the FEA are used to inform the geometry and configuration of the STM, ensuring consistency between numerical results and theoretical modeling. Within this framework, supplementary bar is interpreted as a confinement mechanism that enhances the effective compressive capacity and stability of the concrete struts. This conceptual integration provides the basis for developing a modified analytical expression for anchorage capacity that explicitly incorporates the contribution of the supplementary bar.

1.2. Research Flowchart

The overall research flow chart is illustrated in Figure 3. The research flow begins with the objective of evaluating the anchorage performance of headed bars embedded in exterior BJCs. As a basis for the study, previously reported experimental results by Mohsuni et al. [18] and Mohsuni & Matsui [19] are adopted to provide reference behavior and validation data. Building on this foundation, a 3-D FE model is developed to simulate the anchorage behavior. The numerical model is then validated against experimental results to ensure it accurately reproduces key responses, including load–displacement behavior, cracking patterns, and strain bars. In parallel, an STM is established to represent internal force transfer in the joint. STM formulation is informed by the minimum principal stress trajectories from the FE analysis, which guide identification of compression struts and load paths. STM predictions are validated against both numerical and experimental observations. Following the successful validation of both the FE model and STM, a parametric study is conducted to investigate the influence of supplementary bars, specifically focusing on variations in bar diameter and quantity. The insights obtained from this study are used to quantify the contribution of supplementary bars to anchorage capacity. Finally, based on these findings, an improved modification factor is proposed and incorporated into the modified Kubota and Murakami empirical formula.

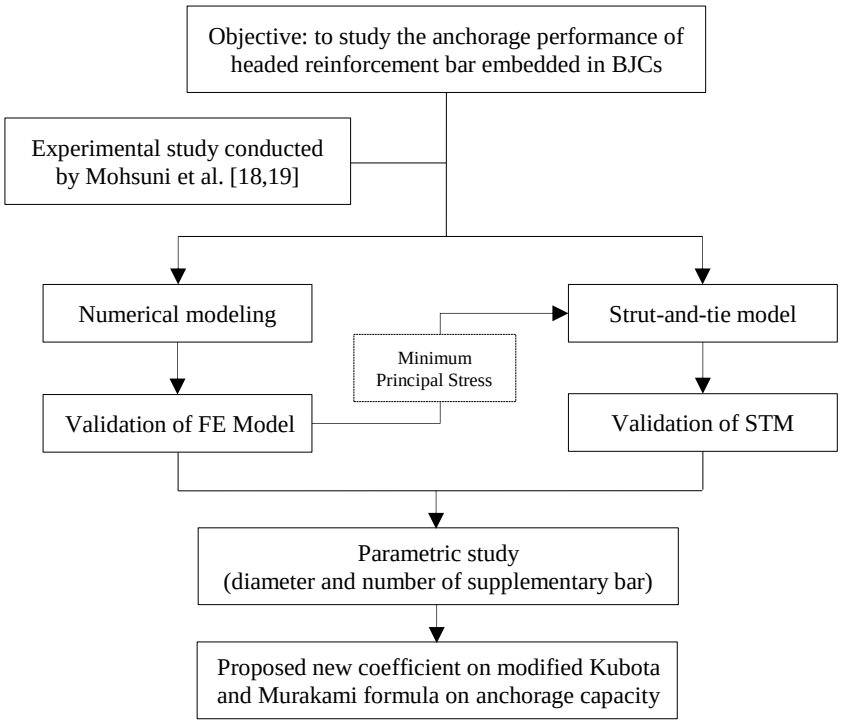

Figure 3. Research flowchart

2. Experimental Programs

2.1. Specimens Detail

Mohsuni et al. [18] and Mohsuni & Matsui [19] performed pullout tests on 70% full-scale roof exterior BCJs to assess the anchorage performance of headed bars. Six specimens with headed bars embedded in L-shaped BCJs were designed and tested. All specimens had identical column dimensions of 540 mm × 540 mm, and the specimen details are summarized in Table 1. Specimen LE25-M was designated as the reference specimen. The headed bars in all specimens served as the primary longitudinal reinforcement of the column. Figure 4 illustrates the standard cross-section of specimen LE25-M. The investigated parameters included the diameter of the headed bar, the embedment length, and the diameter of the supplementary bars. The selected diameters and embedment lengths correspond to realistic reinforcement detailing used in BCJs and were intentionally chosen to reproduce typical anchorage conditions while ensuring the occurrence of governing failure modes such as concrete cone failure and side blowout. The supplementary bar parameters were defined to systematically vary the reinforcement ratio (ρ_s), including values below and above the design requirement (0.2%), as specified in the AIJ Standard Structural Design Criteria, thereby enabling evaluation of confinement effects. The only difference between specimens LE25-Ma and LE25-M was the diameter of the supplementary bar: a 6 mm bar was used in LE25-Ma, whereas a 13 mm bar was used in LE25-M. Specimens LE19-M, LE25-M, and LE32-M were designed with different headed-bar diameters and concrete covers while maintaining the same embedment length of 375 mm. In contrast, specimens LE25-S, LE25-M, and LE25-L had identical head-bar diameters (25 mm) and concrete covers (68 mm) but different embedment lengths, classified as short, medium, and long, respectively. The maximum embedment length of 450 mm was adopted for specimen LE25-L, while the minimum embedment length of 300 mm was used for specimen LE25-S. All specimens were designed to develop failure modes, such as concrete-cone failure or side blowout. Table 2 lists the dimensions of the plate nut corresponding to Figure 5.

Table 1. Specimens detail

Specimen	Beam-column joint $b \times D$ (mm)	Headed bar n-d_h	Concrete cover C (mm)	Effective depth l_d (mm)	Supplementary bars n-d_s
LE25-M	540 × 500	2-D25	68	375	4-D13
LE25-Ma	540 × 500	2-D25	68	375	4-D6
LE25-S	540 × 500	2-D25	68	300	4-D13
LE25-L	540 × 575	2-D25	68	450	4-D13
LE19-M	540 × 500	2-D19	60	375	4-D13
LE32-M	540 × 500	2-D32	70	375	4-D13

Note: b and D denote the width and depth of the joint, respectively; d_h is the diameter of the headed bar; l_d is the embedment length of the headed bar; n is the number of bars; C is the distance between the side face of the concrete and the center of the bar; and d_s is the diameter of the supplementary bar.

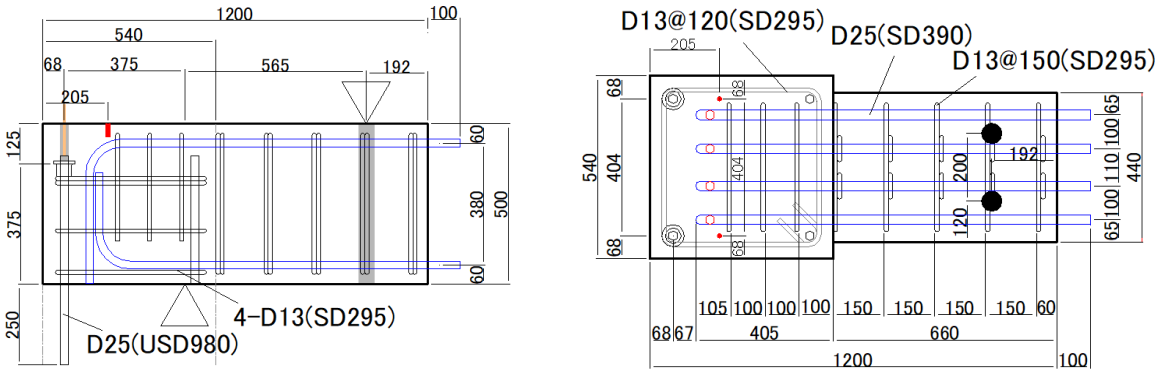

Side view *Plan view*

Figure 4. Cross-section and detail of the LE25-M Specimen

Table 2. Dimension properties of plate nut

Rebar diameter (mm)	R1 (mm)	B (mm)	C (mm)	t (mm)	L (mm)
D19	50	32	36	7	47
D25	65	41	46	9	59
D32	80	50	54	11	76

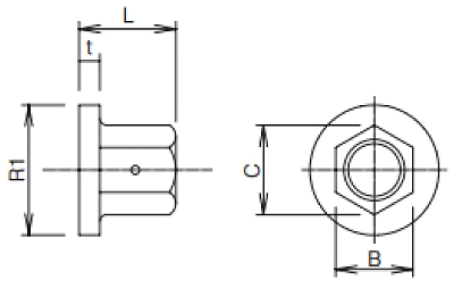

Figure 5. Plate-nut detail

2.2. Material Properties

Table 3 lists the concrete material properties based on compression and splitting tests. Table 4 lists the material properties of the reinforcing bars. A high-strength SD980 reinforcing bar was used for the headed bars to prevent bar fractures. Grade FCAD 1200-2 steel, with a yield stress of 900 N/mm^2 and a tensile strength of 1200 N/mm^2 or higher, was used for the plate nuts, in accordance with the Japan Industrial Standard.

Table 3. Material properties of concrete

Specimen	Compressive strength σ_B (N/mm^2)	Tensile strength f_t (N/mm^2)	Elastic modulus E_c (N/mm^2)
LE25-M	33.2	2.8	27900
LE25-Ma	32.6	2.8	27800
LE25-S	33.1	3.2	27300
LE25-L	33.6	2.8	25200
LE19-M	30.9	2.6	28200
LE32-M	32.7	3.2	28100

Table 4. Material properties of reinforcement bar

Reinforcement bar	Yield stress σ_y (N/mm^2)	Young modulus E_s (N/mm^2)	Tensile strength f_t (N/mm^2)	Remark
D6 (SD295)	407	195000	531	Supplementary bar
D13 (SD295)	342	193000	463	Supplementary bar
D25 (SD390)	441	196000	611	Beam main bar
D32 (SD390)	436	198000	620	Beam main bar
D19 (USD980)	1093	195000	1161	Headed bar
D25 (USD980)	1095	194000	1165	Headed bar
D32 (USD980)	1098	196000	-	Headed bar

2.3. Test Setup

Figure 6 depicts the schematic and photo of the loading setup employed during the test. The reaction force was transmitted to the force application beam, while each headed reinforcing bar was subjected to axial tensile loading applied directly through a centrally aligned hydraulic jack with a capacity of 500 kN. Displacement gauges were mounted on the upper surface of the plate nut to record the withdrawal displacement of the headed bars, as illustrated in Figure 7. Test results demonstrated that the anchorage capacity of the headed bars was significantly influenced by the presence of supplementary bars. These supplementary bars enhanced the diagonal compressive stress distribution within the concrete matrix, thereby increasing its resistance against the applied pullout forces. Therefore, ensuring enough supplementary bars is critical to optimize anchorage performance.

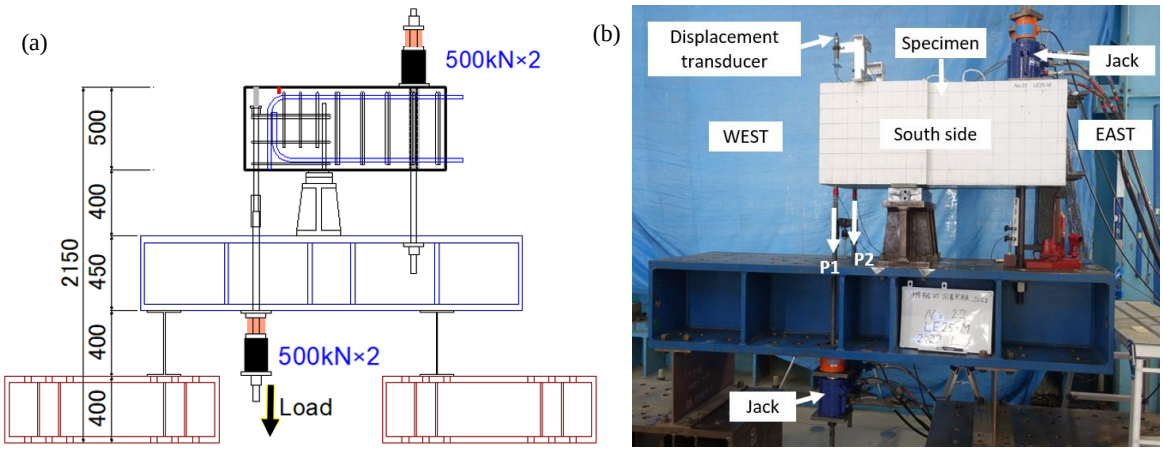

Figure 6. (a) Schematic illustration and (b) photo of test setup [18]

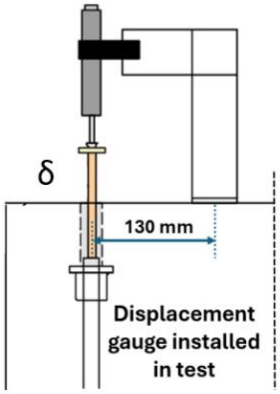

Figure 7. Position of displacement gauges

3. Finite Element Analysis

To uncover the internal force-transfer mechanism that cannot be directly observed from experiments, numerical simulation is first employed as an investigative tool.

3.1. Element Used

FINAL v11 [21] software was used for non-linear FE analysis of the BCJ specimens. The analysis was three-dimensional, assuming a triaxial stress field. Concrete was modeled with 8-node hexahedral elements, and reinforcing bars with 1D line elements. Headed bars were represented by 4-node quadrilaterals. Slippage between main-headed bars and concrete was simulated using a 4-node interface element, which defined the bond-slip relationship between concrete and steel. At the plate nut interface, nodes on the top plate nut were detached from concrete nodes, while those on the bottom were directly connected.

3.2. Material Constitutive Model

The modified Ahmad model was used to calculate the concrete compressive stress-strain relationship in the FE model [22]. Based on fracture energy, the Nakamura-Higai model [23] was used to model the stress-decrease region, as shown in Figure 8-a. The Ottosen four-parameter model is used for fracture conditions under triaxial stress. The crack-softened

area on the tension side was assumed to bear almost no tensile stress after cracking, and strain reduction after cracking was not considered. The tension stiffening characteristic by the Izumo et al. [24] model was used (Equation 1), and the coefficient *c* was set to 1.0, assuming that almost no tensile stress is borne after cracking.

$$\frac{\sigma_t}{\sigma_{cr}} = \left(\frac{\varepsilon_t}{\varepsilon_{cr}}\right)^C \quad (1)$$

where, σ_t is the tensile stress of concrete, σ_{cr} is the tensile strength under biaxial loading, ε_t is the tensile strain in the direction perpendicular to the crack, ε_{cr} is the tensile strain when crack occurs, and *c* is a factor of the tension stiffening phenomenon.

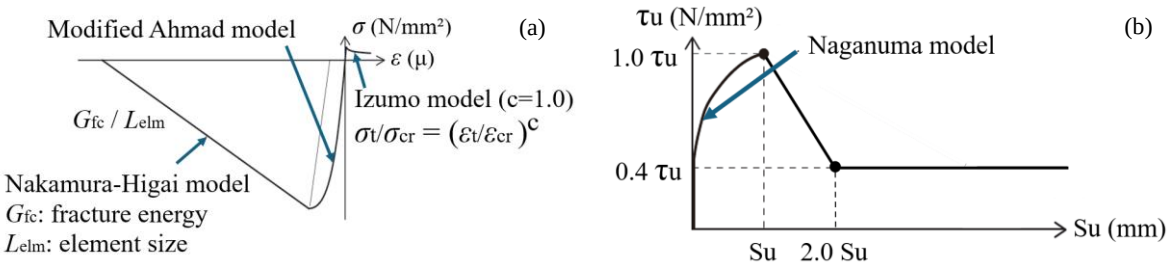

Figure 8. (a) Principal stress equivalent uniaxial strain relation of concrete and (b) Bond stress-slip relationship

The shear transfer model after cracking on the beam was based on the Naganuma model [25], while the joint was assumed to have no shear transfer (zero shear stiffness). The factor for reducing compressive strength after cracking in the FE model was Collins et al.'s proposed formula [26], while the LE25-Ma model used Naganuma's proposed formula [25]. The slip of the headed reinforcing bars was modeled by inserting joint elements. The bond characteristics between headed reinforcing bars and concrete were based on the model by Naganuma et al. [27], and a slip of 1.0 mm at the maximum bond stress was assumed. Then, peak stress (τ_u) was calculated based on *fib* Model Code 2010 [28], as follows:

$$\tau_u = 2.5\sqrt{f_{cm}} \quad (2)$$

where, f_{cm} is the mean of compressive strength of concrete. Figure 8-b shows the bond stress and slip relationship between reinforcing bars and concrete. The bond between the transverse reinforcement and concrete is assumed to be perfectly bonded. The model was designed so that only the area corresponding to the BCJ panel cover was brittle. The stress-strain relationship adopted to represent reinforcement bar behavior was the modified Menegotto-Pinto model. The plate at the support was modeled as a perfectly elastic body with a Young's modulus of 2.05×10^5 N/mm^2.

3.3. Loading and Boundary Condition

To simulate the test setup in the FE model, boundary conditions were applied to a specific plane, as shown in Figure 9. Specifically, in this analysis, the pin support at point A was restrained in the z direction only, while the support at point B was fixed in the x and z directions. Next, a downward displacement-controlled load was applied at the lowest node of the headed reinforcement (point C) to a displacement of 50 mm. The analysis ended when the specified step value was reached. Finally, separate nodes were defined for the concrete and the anchor plate to measure and reproduce the pull-out displacement at the anchor plate.

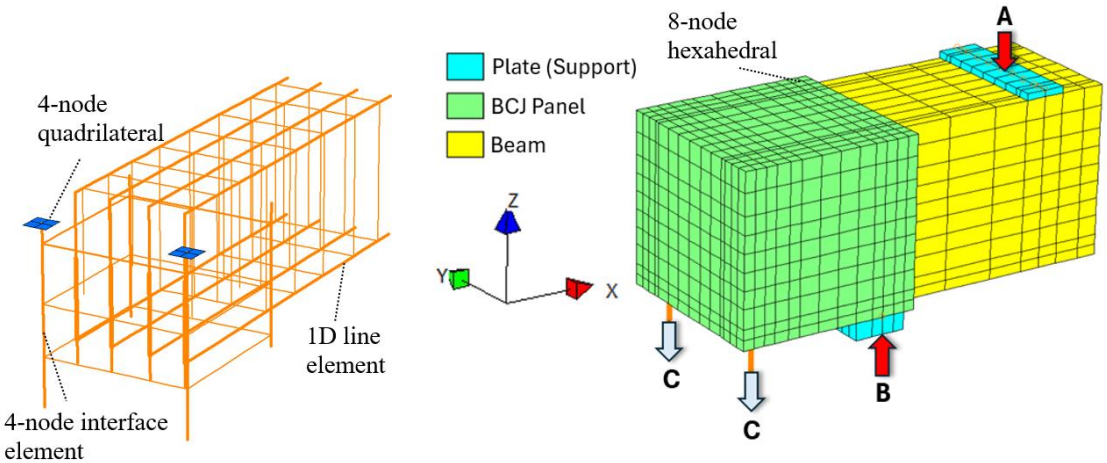

Figure 9. The 3D FE model and boundary condition of the specimen (LE25-M) developed in FINAL

3.4. Validation of FE Model with Test Results

A comparison between numerical results and the test specimens was conducted to evaluate the ability of the developed FE simulation to estimate the concrete breakout strength of headed bars in roof exterior BCJs. Because the test results indicate that the use of supplementary bars significantly influences the anchorage capacity of the headed bars, and this study aims to propose a modification factor that accounts for the effect of supplementary bars, furthermore, the validation of the FE analysis is limited to comparisons with experimental results from specimens with different supplementary bar conditions (LE25-M and LE25-Ma).

3.4.1. Pullout Load vs. Displacement Response

The comparison of the pullout load and displacement curves obtained from both the FEA and the tests for LE25-M and LE25-Ma is presented in Figure 10-a. The pullout displacement (δ) in the FEA was calculated as the difference between the displacements at nodal points A and B ($\delta = \delta_A - \delta_B$), as illustrated in Figure 10-b. The LE25-M model, with a larger hoop diameter, exhibited higher peak load than LE25-Ma. Notably, even after the appearance of diagonal cracks, LE25-M continued to increase its pullout load due to its greater anchorage strength. The gradual increase in load after initial cracking indicates that the supplementary reinforcement effectively delays crack propagation by providing lateral confinement to the concrete. In contrast, LE25-Ma, having a lower anchorage capacity, experienced a significant drop in pullout load following the formation of diagonal cracks. The rapid post-peak load drop suggests insufficient confinement, leading to unstable crack growth and reduced residual capacity. LE25-Ma model demonstrated a particularly close match between the numerical prediction and test results until the end of pullout displacement.

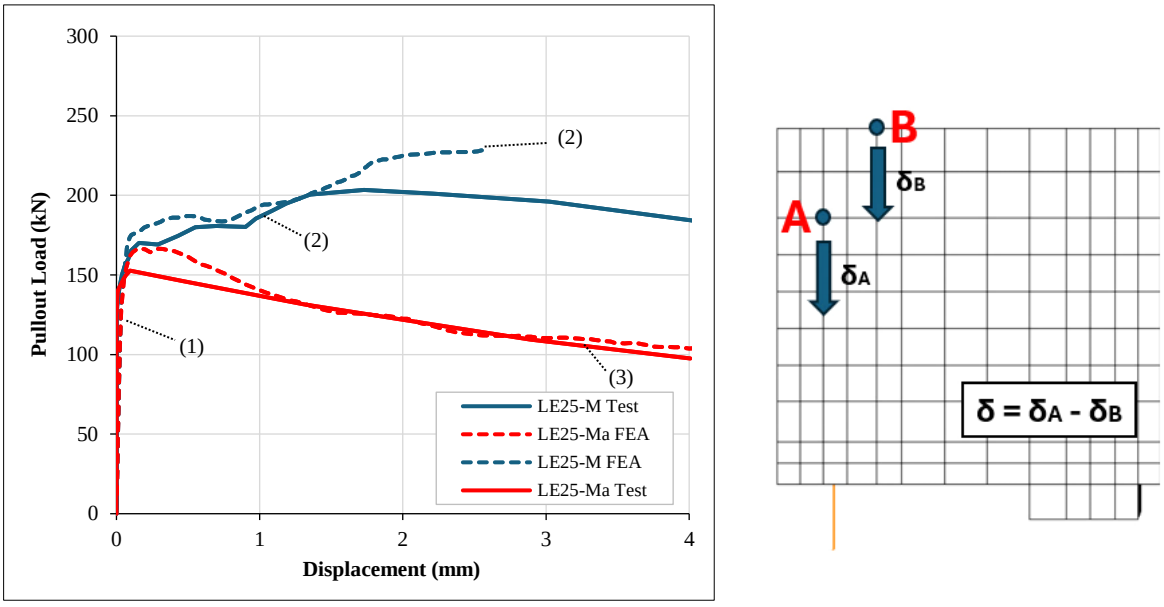

(a) (b)

Figure 10. (a) Pullout load-displacement relationship of LE25-M and LE25-Ma; (b) Displacement calculated for FE analysis

Overall, the FE models align very well with the experimental result, particularly in terms of initial stiffness and the development of pullout load, up to displacements of 1.5 mm for LE25-M and 4 mm for LE25-Ma. This behavior confirms that supplementary reinforcement plays a critical role not only in increasing ultimate strength but also in improving the overall ductility and stability of the anchorage system.

3.4.2. Failure Mechanism (Crack Pattern)

Validation of the crack pattern in concrete is necessary to assess the potential for undesirable tensile load effects arising from rapid crack formation due to headed bar pullout. Figure 11 compares crack patterns on the concrete in LE25-Ma between the test and FEA results. The number sign in Figure 11 corresponds to Figure 10 (a). The failure mechanism in the experiment and FEA was as follows: (1) a vertical crack first emerged from the bottom of the BCJ panel region along the headed bar, around 75 mm, and (2) as the load increased to reach the peak load, diagonal cracks began to appear around the anchorage bar. The comparison of crack angles between the FE and test results

is calculated as the average of the three-line cracks (a, b, and c), as shown in Figure 11. The crack occurred in the FEA, and the test angles were 45° and 44°, respectively. It is indicated that the development of diagonal cracks and concrete spalling in the FE model is consistent with the test results. (3) Finally, further diagonal cracks appeared in the BCJ panel, and the pullout displacement of the anchorage bar began to occur. When diagonal cracks also appeared near the support plate, the pullout load of the headed bar decreased further. Both the FEA and test results indicate that cone cracking occurred in the concrete cover, leading to ultimate failure. The failure process of the LE25-M model is similar to that of the LE25-Ma model. Overall, the close agreement between test observations and FEA results confirms that the numerical model accurately captures the crack development and failure mechanism associated with the headed bar pullout.

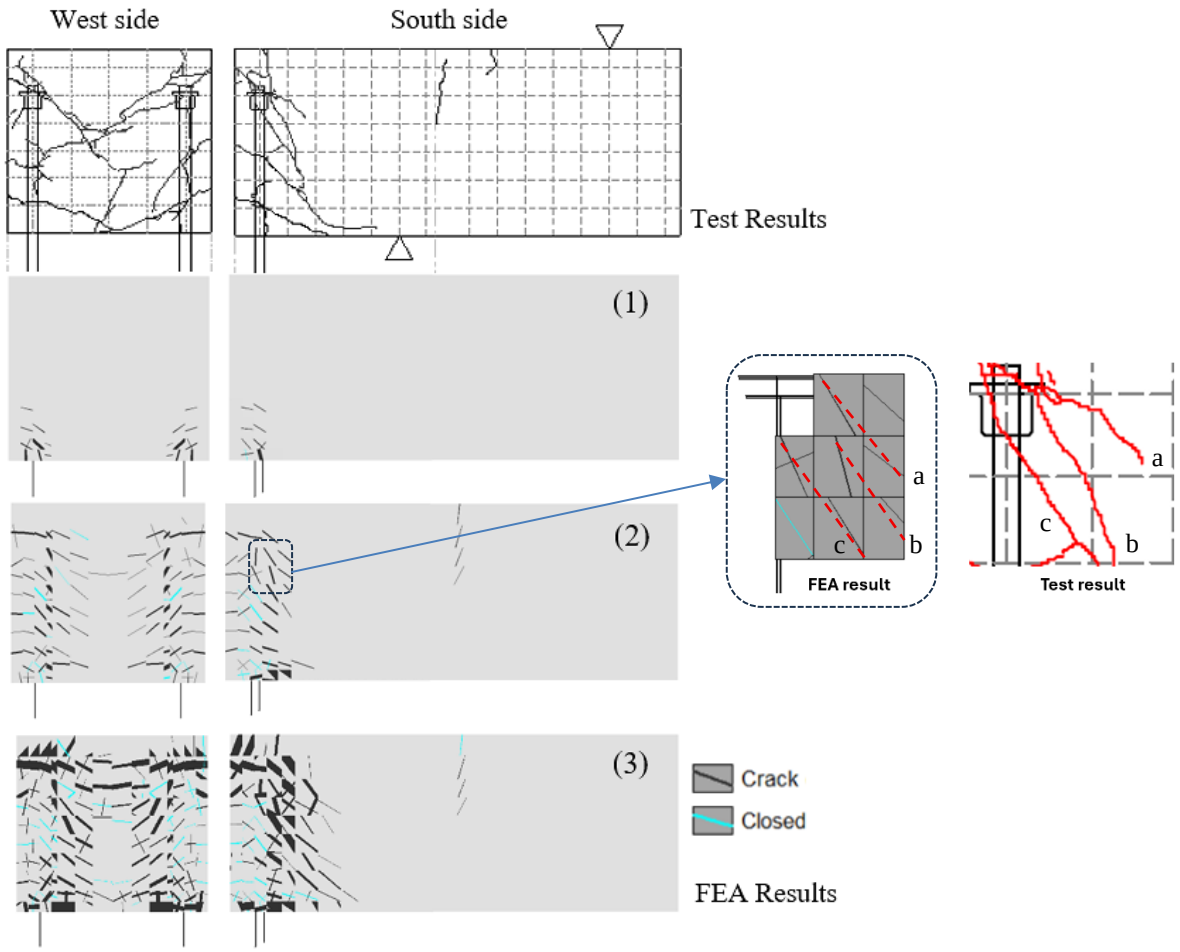

Figure 11. Crack patterns of LE25-Ma specimen and the FE model

3.4.3. Strain of Reinforcing Bars

Figure 12 presents the relationship between pullout load and strain for both supplementary and main beam bars in the LE25-Ma model. Figure 13 shows the locations of the strain gauges on specimens where strain measurements were taken for comparison with the FEA. The strain distribution in the supplementary bar provides further insight into the load-transfer mechanism. Both test and FEA results show that higher strain values observed in the topmost supplementary bars (a5) indicate that these bars actively participate in resisting the tensile forces induced by the pullout action. This confirms that the supplementary bar is not merely a passive confinement but contributes directly to force transfer through tension ties. Notably, the supplementary bars exhibit higher strain readings at points a3 and a5 than the test results. The strain at a5 in the FEA exceeds the yield strain limit ($\mu = 2087$). The discrepancy between experimental and FE strain values may be attributed to idealized bond conditions and material modeling assumptions in the numerical simulation. The strain at point a1 indicates compression of the supplementary bar under the pullout load in both the test and the FEA. In the main bar, both the test and the FEA show that the strain at point b1 is higher than at b2, while the FEA results underestimate the test results. This proves that the strain in the supplementary bars is influenced by the shape of the concrete cone. These observations confirm the FE model's ability to replicate the strains observed experimentally in the reinforcing bars.

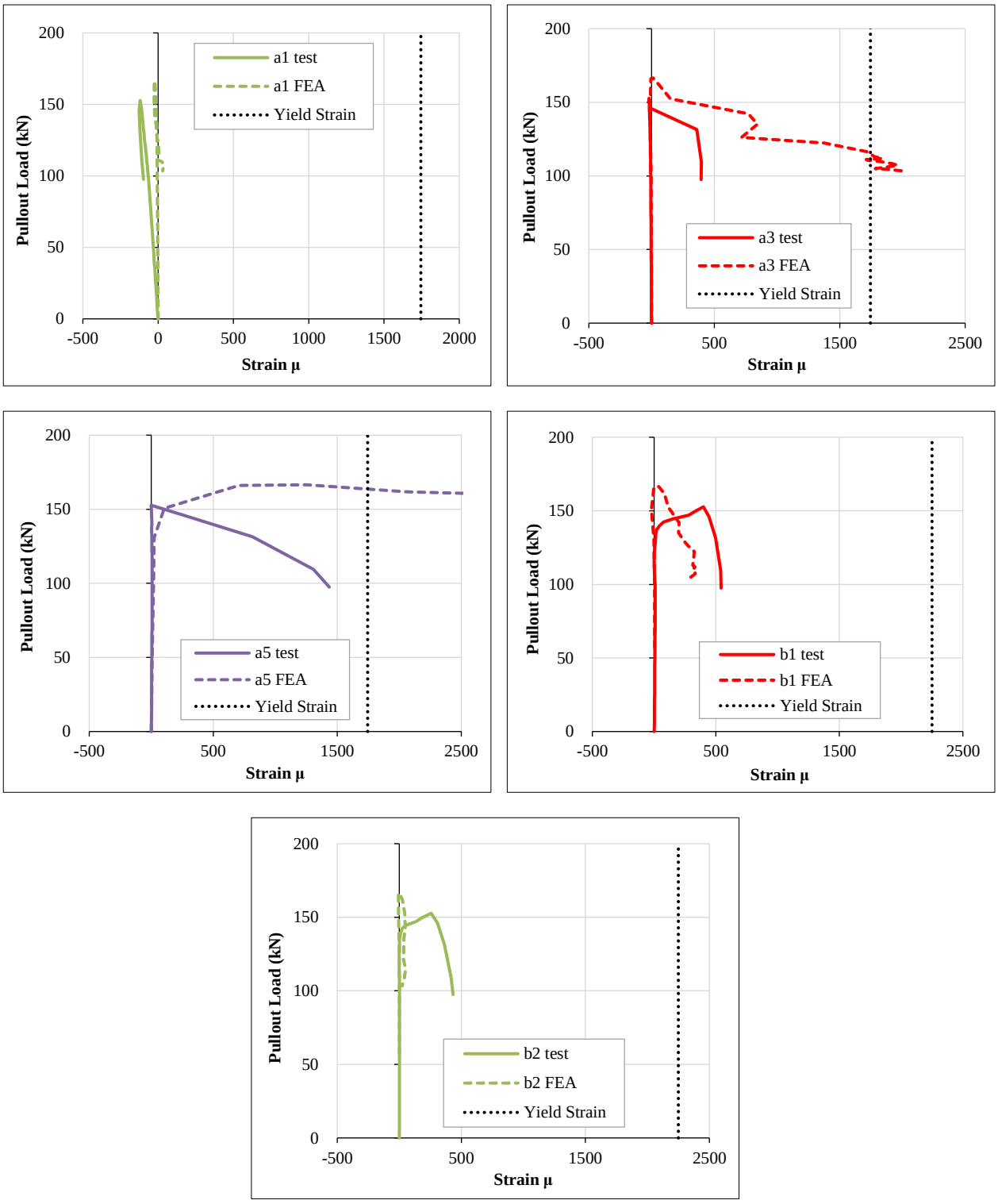

Figure 12. Relationship between load and strain of supplementary and main beam bars of LE25-Ma

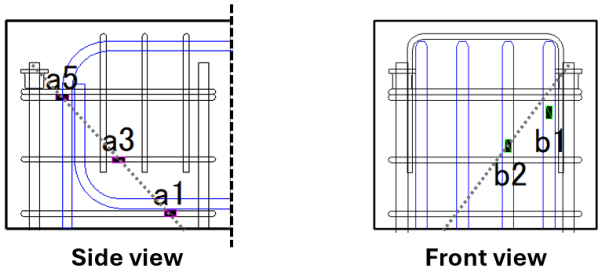

Figure 13. Strain gauges position of LE25-Ma

3.4.4. Minimum Principal Stress

Figure 14-a illustrates the minimum principal stress distribution obtained from the FE analysis at peak load for LE25-M and LE25-Ma, while Figure 14-b illustrates the cutaway diagram highlighting the positions of the headed and supplementary bars. The stress contour shown in the figure is observed at the pullout load indicated as (2) in Figure 10(a). The initial cracks in the analysis tend to be inclined, concentrating at the base of the headed reinforcing bar, where cracking first occurs. The stress then propagates at a 45-degree angle from the plate nut of the headed reinforcement bar. This concentration of stress can lead to crack initiation at the anchorage region of the headed bars. A clear concentration of compressive stress can be observed along diagonal paths extending from the headed bar toward the surrounding concrete, indicating the formation of compression struts.

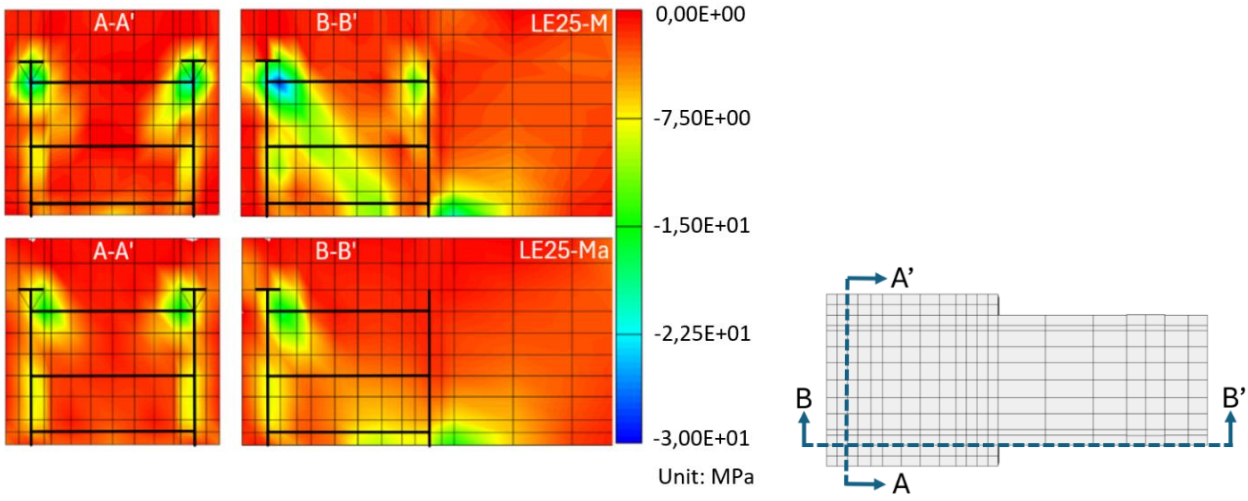

Figure 14. (a) Minimum principal stress of LE25-M and LE25-Ma model; (b) Cutaway of LE model

As the diameter of supplementary reinforcement increases, the width of the compression strut becomes larger, allowing higher compressive forces to be sustained before failure. Both FE models show that the concentration of compressive stress near the plate nut and top supplementary bar indicates that these regions act as critical load-transfer zones. It also indicates that the presence of supplementary bars is important for resisting bearing forces in concrete and increasing the concrete breakout capacity. These findings confirm the stress state at the time of fracture, with the concentrated stress in the FE model aligning well with the observed specimen failures. These stress trajectories provide direct evidence of the internal force-transfer mechanism and serve as the basis for the strut-and-tie model presented in this study.

3.5. Parametric Study on FE Analysis

The numerical results showed that the proposed FE model adequately describes the behavior of the headed bar under pullout loading. In addition, a parametric numerical study was conducted to investigate the influence of supplementary bar parameters on the pullout capacity of the anchors, including diameter and number of supplementary bars, that have different supplementary bar ratios (ρ_s). The supplementary bar parameters were selected to represent a practical range of reinforcement ratios commonly used for confinement in BCJs. The chosen configurations enabled controlled variation of ρ_s, which is the primary variable introduced in this study. This range was sufficiently broad to capture both low and high confinement conditions and enable the derivation of a regression-based coefficient for improving existing empirical formulations. The ρ_s was calculated as follows:

$$\rho_s = \frac{\sum A_s}{A_c} \tag{3}$$

where, ΣA_s is the total cross-sectional area of supplementary bars in the beam-column joint, and A_c is the effective core area confined by the supplementary bars ($b_c \times d_c$). The definition of the effective confined area used to calculate the supplementary reinforcement ratio is illustrated in Figure 15. b_c and d_c are the effective width and depth of the core, respectively. Notably, the models on this parametric study were designed based on the specimen LE25-M. In this section, LE25-M and LE25-Ma are renamed to E4-13 and E4-6, respectively.

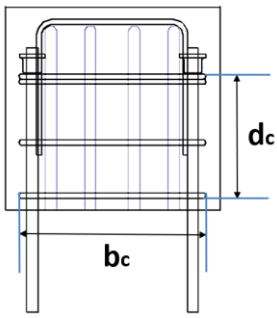

Figure 15. The effective area confined by the supplementary bars

The effect of supplementary bar diameter (d_s) on the concrete breakout strength of headed bars embedded in BCJ was investigated by modeling E4-10, E4-16, and E4-19 with d_s values of 10 mm, 16 mm, and 19 mm, respectively. Models with larger bar diameters provided better resistance to the applied pullout load. However, the rate of capacity increase is relatively moderate, indicating that diameter alone is not the dominant parameter governing anchorage strength. As shown in Figure 16-a, increasing the diameter to 16 mm and 19 mm resulted in higher ultimate concrete breakout capacities, by 9.8% and 11.4%, respectively, compared to the capacity of E4-13. The E4-10 model showed a decrease in anchorage capacity of around 7.4%, as shown in Table 5. The crack patterns and failure modes of E4-10, E4-16, and E4-19 are the same as those of E4-13.

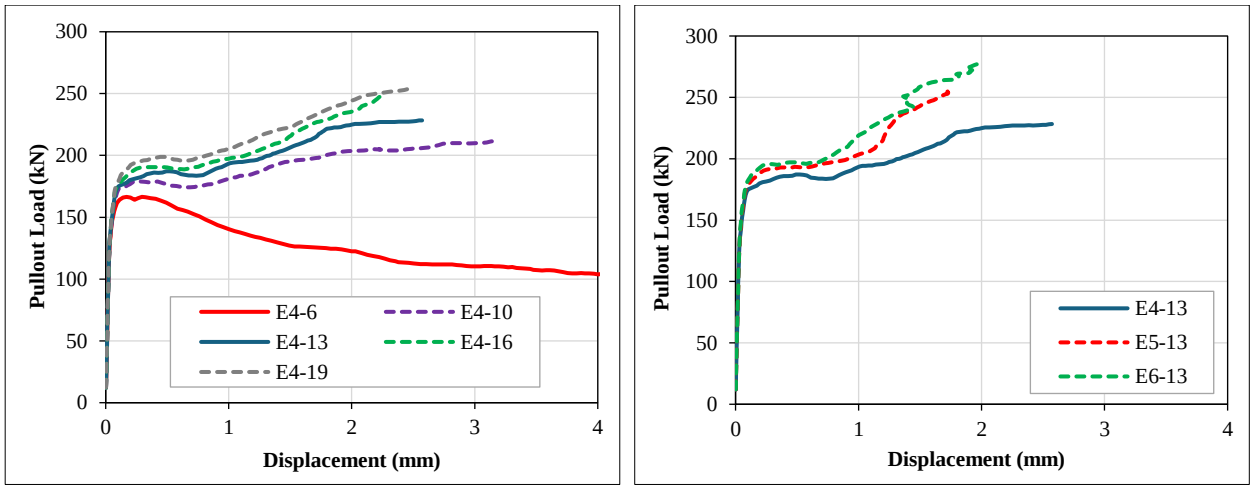

(a) (b)

Figure 16. Pullout load-displacement relationship of supplementary bar variable: (a) diameter and (b) number

Table 5. FE parametric study results

Model	Variable	Ratio of supplementary bar (%)	Max. Pullout Capacity (kN)	Percentage of Increase (%)
E4-6	d_s = 6 mm	0.134	166.5	-27.1
E4-10	d_s = 10 mm	0.316	211.4	-7.4
E4-13	d_s = 13 mm	0.540	228.3	-
E4-16	d_s = 16 mm	0.810	250.7	9.8
E4-19	d_s = 19 mm	1.142	254.3	11.4
E5-13	n_s = 5	0.668	257.2	12.6
E6-13	n_s = 6	0.802	278.1	21.8

Varying the number of supplementary bars (4, 5, and 6) was considered to study their effect on the concrete breakout strength capacity of headed bars. The arrangement of supplementary bars in this parametric model is shown in Figure 17. The measured ultimate pullout capacity is plotted against the varying number of supplementary bars of the headed bar in Figure 16-b. The figure shows that increasing the number of supplementary bars results in a more pronounced increase in anchorage capacity. A 12.6% increase in pullout capacity was observed when the number of supplementary bars increased from 4 to 5, whereas an increase of 21.8% was observed when the number increased from 4 to 6. This observation suggests that the distribution and density of confinement are more critical than individual bar size.

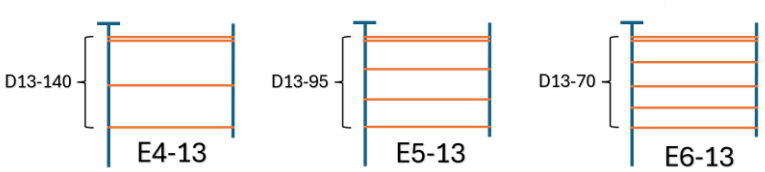

Figure 17. Configuration of parametric study on supplementary bar number variation

The results of the parametric study demonstrate that the influence of supplementary bars is governed primarily by its contribution to confinement and strut formation. From a mechanistic perspective, the improvement in anchorage performance can be explained by the interaction between the concrete struts and the confining action of the supplementary bar. As the bar ratio increases, the tensile stresses induced by crack development are more effectively resisted, resulting in a more stable load-transfer mechanism. In particular, the supplementary reinforcement provides lateral restraint to the surrounding concrete, limiting crack opening and suppressing the propagation of splitting cracks along the anchorage zone. This confinement effect enhances the integrity of the concrete struts, allowing them to sustain higher compressive stresses without premature degradation. Furthermore, the improved supplementary bar ratio promotes a more uniform stress distribution around the anchored bar, reducing stress concentrations that would otherwise lead to localized failure.

Increasing the diameter of the supplementary bars enhances the stiffness of the confinement system, resulting in a modest increase in anchorage capacity. However, increasing the number of supplementary bars has a more pronounced effect, leading to the formation of multiple load paths and additional diagonal compression struts. This significantly improves the efficiency of force transfer and delays the onset of concrete cracking.

4. Strut and Tie Model

Based on the mechanistic insights obtained from the FE analysis, a strut-and-tie model (STM) is developed to idealize the internal force flow and provide a simplified yet physically consistent representation of the anchorage mechanism. STM is the simplest method for distributing the applied load as a truss in concrete BCJs reinforced with headed bars. The member that transfers the tension force is called the tie, while the strut represents the members that transfer the compression forces. This part of the study was conducted using the STM, in accordance with ACI 318-19 [29], for the design of struts, ties, and nodes. STM was developed for the tested specimens to facilitate understanding of internal force flow based on the identified probable failure mechanisms [30]. The model represents the structural member as an idealized truss system contained within its boundaries.

4.1. Model and Assumption

In this study, 3D STM was employed to predict the pullout capacity of headed reinforcement bars and the cross-sectional area of the primary strut, based on the concrete-cone failure mechanism observed in both experimental testing and FEA. An optimization procedure was implemented to identify an STM configuration that yields acceptable strength predictions. The STM design procedure comprised the following steps:

- Define the boundaries of the D-region and determine the applied sectional and local forces.
- Develop a truss model for the BCJ panel of the LE25-M specimen based on the stress distribution obtained from the FEA (STM geometry determination). To simplify, the model represents only a one-headed bar, since the specimen is symmetric.
- Identify the governing failure location and assume the initial failure mechanism. In this study, it was assumed that the primary strut formed between the top supplementary bar and the headed bar reached its limiting compressive strength first.
- To provide the assumption of the effective width of main strut element through which the strut passes (b_{strut}), the model of LE25-M was analyzed first. By inputting the maximum experimental pullout load on the truss model, the internal forces in the compression and tension members were calculated using linear elastic analysis. The internal force of main strut (strut DA) was used to propose cross-sectional areas (W_{strut} x b_{strut}) of the main strut.
- Propose an equation for b_{strut}, as presented in Equation 8.
- Validate Equation 8 by calculating the axial forces of the STM members and the corresponding pullout loads for another set of specimens (LE25-Ma, LE25-S, LE25-L, LE19-M, and LE32-M). In this step, the C_{strut} was decided first by using Equations 4 to 8, then the pullout load was obtained from the truss analysis.
- Conduct a parametric study with variation of diameter and number of supplementary bars.

Figure 18 shows the principal stress trajectories used to define the STM geometry, while Figure 19 presents the idealized STM for LE25-M. Solid blue lines indicate tensile members, solid red lines indicate main compressive struts, and dashed red lines indicate additional compressive struts. The STM was developed based on these assumptions: Headed reinforcement bars (T_{DE} and T_{EF}) and top and middle supplementary bars (T_{DC} and T_{EB}, T_{DH} and T_{DI} for the x- and y-axes) in the BCJ panel resist tensile forces. Each tie is placed at the centroid of its corresponding reinforcement. The bottom supplementary bar was not included because it was in compression, as observed in the test and FEA results.

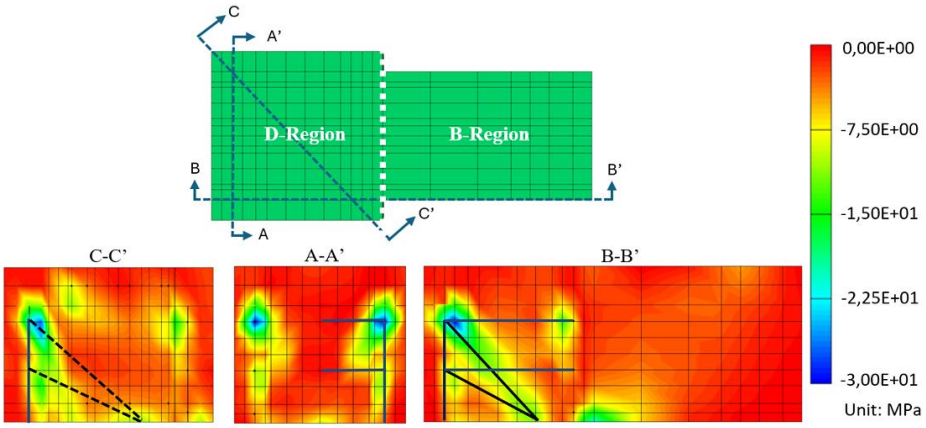

Figure 18. Minimum principal stress of LE25-M at max pullout capacity

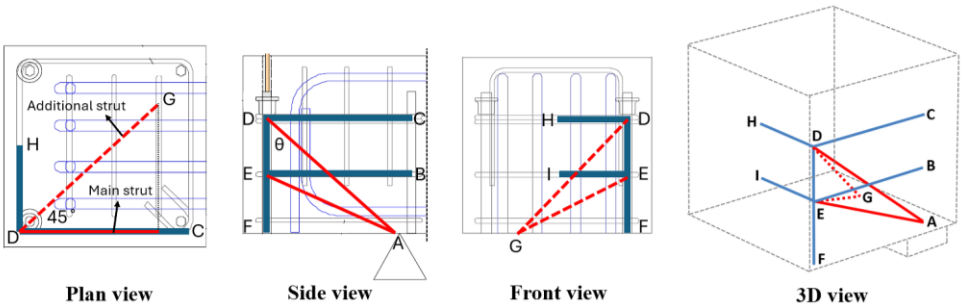

Figure 19. STM basic model of LE Specimen

The main struts, DA and EA, are between the headed bar and the top and middle supplementary bars. Strut DG is at a 45° angle from the top supplementary bar along the x and y axes. This additional strut was added to account for the concrete bearing force at the plate nut. Strut EG addresses stress concentration between the middle supplementary bars along the x- and y-axes. Nodes A and G, namely Compression-compression-compression (CCC nodes), are located at the centroid of the beam's bottom bars. Nodes D and E, namely Compression-compression-tension (CCT nodes), are located at the intersections of the headed bar axes with the top and middle supplementary bars, respectively. As per AASHTO LRFD [31], the angle between a strut and tie should be over 25°.

The effective compressive strength used to determine the strut depth was taken as 85% of the concrete compressive strength [32], with the strut condition determined according to ACI 318-02 (βs = 0.60) [2]. The compression force in a strut is calculated as follows:

$$f_{cu} = 0.85 \, . \beta_s . Fc \tag{4}$$

$$C_{strut} = f_{cu} . W_{strut} \, . b_{strut} \tag{5}$$

where, W_{strut} denotes the width of strut, C_{strut} is the compression force of a strut, Fc is the concrete strength, and b_{strut} is the width of each element that the strut goes through. Some codes (AASHTO Code [31], the Ontario Bridge Code [33], and the CSA Canadian Concrete Building Code [34]) all allow the node boundary to be drawn up to six bar diameters ($6d_h$) from the surface of the tie reinforcement. In this study, the W_{strut} was assumed to be based on the codes were chosen as follows:

$$W_{strut} = l_a \sin\theta \tag{6}$$

$$l_a = 2 \, (h_n + d_s) \tag{7-a}$$

where, l_a is the length of the strut along the headed bar, θ is the angle between strut DA and headed bar, and h_n is the height of the plate nut. A different treatment was applied to the model with the plate nut height greater than half the

clear space between the top and the adjacent supplementary bar ($h_n > 0.5s_s$). To prevent the CTT nodes between adjacent struts from overlapping, l_a was calculated as follows:

$$l_a = 2\ (0.5\ s_s + d_s) \tag{7-b}$$

where, s_s is the clear space between supplementary bar.

Figure 20 shows the assumed main strut dimension used in the model. In this study, STM focuses only on the cross-sectional area of the main strut, which is influenced by the diameter of the headed and supplementary bars. The tensile yielding of the top supplementary bar, T_{DC} and T_{DH}, is not considered because, at maximum pullout capacity, the top supplementary bar still did not reach yielding, as observed in the test and FEA.

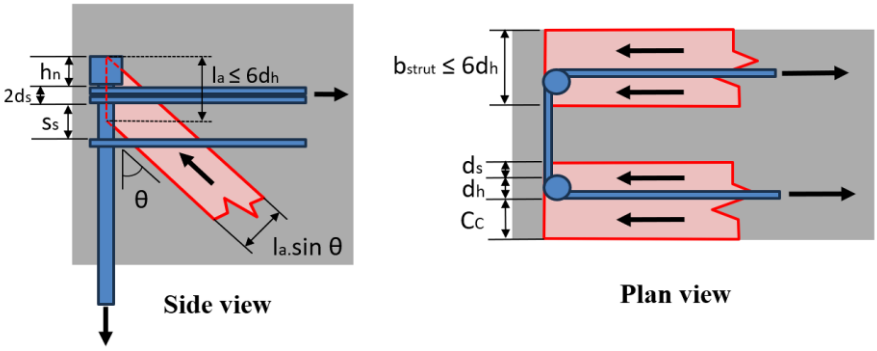

Figure 20. Main strut dimension (CTT node)

Since LE25-M is the benchmark model, the first step is to determine the strut DA capacity required to resist the pullout load applied at the ends of the headed reinforcement bars. The main strut capacity (C_{strut} DA) was calculated by inputting the maximum pullout load at the test result (203.8 kN) on the truss model. From the truss analysis, the C_{strut} obtained was 136.6 kN. By using Equation 4, the cross-sectional area of the main strut (W_{strut} and b_{strut}) was calculated. In this study, W_{strut} was fixed because it is limited by the height of the plate nut (h_n) or the clear spacing between supplementary bar (s_s), while b_{strut} was treated as a flexible value ($\leq 6\ d_h$). From the calculation using Equations 3 to 6, b is calculated to be 93.1 mm. This value of b is acceptable according to the following equation:

$$b_{strut} = C_C + d_h + d_s \tag{8}$$

where, C_C denotes the clear concrete cover (distance from concrete surface to headed reinforcement bar surface), and d_h is the diameter of the headed reinforcement bar. The b_{strut} at the confined part of the BCJ panel is assumed to be shallow because it is replaced by adding strut DG. By using Equation 7, the value of b_{strut} was recalculated (b_{strut} = 93.5 mm), and used to design the C_{strut}. The predicted pullout capacity was then calculated based on the target C_{strut}, as shown in Table 6. To validate Equation 7, the STM was also applied in another model. For the specimens with different embedment lengths (LE25-S and LE25-L), there is a difference in the angle of strut DA due to the distance between headed bar and the BCJ panel support. It is also confirmed that the diagonal crack propagation of that specimen is more sloping and steeper for LE25-S and LE25-L, respectively, than LE25-M, as shown in Figure 21.

Table 6. Technical parameters used for Strut DA

No.	Technical Parameter	Unit	LE25-M	LE25-Ma	LE25-S	LE25-L	LE19-M	LE32-M
1	Angle θ	°	45	45	50	40	45	45
2	C	mm	55.5	55.5	55.5	55.5	50.5	54
3	d_h	mm	25	25	25	25	19	32
4	d_s	mm	13	6	13	13	13	13
5	b_{strut}	mm	93.5	86.5	93.5	93.5	82.5	99
6	l_a	mm	122	108	122	122	122	122
7	W_{strut}	mm	86.3	76.3	90.7	81.6	86.3	86.3
8	C_{strut}	kN	136.6	109.8	143.1	130.8	112.2	142.4

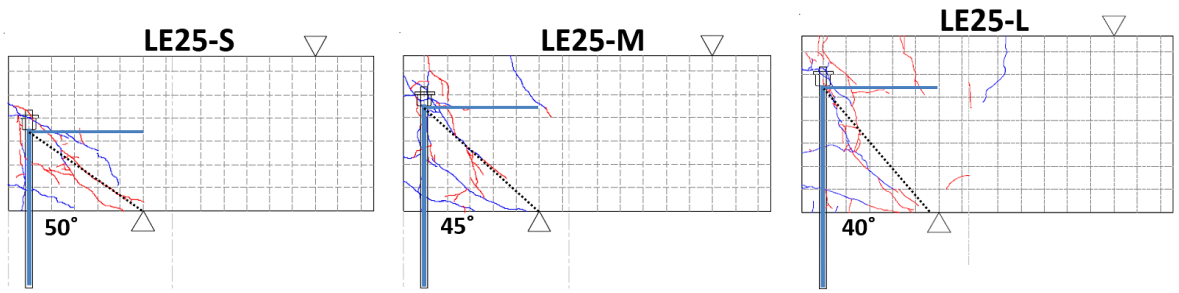

Figure 21. Diagonal crack pattern angle of specimens with different embedment length

4.2. Validation of STM

Table 7 and Figure 22 compare the pullout capacities of headed bars obtained from experimental testing and STM predictions. The STM predictions show good agreement with the experimental results, with the P_{STM}/P_{Exp} ratio ranging from 0.964 to 1.077. For most specimens, including LE25-M, LE25-S, LE25-L, and LE19-M, the STM predictions differ from the experimental values by less than 2%, demonstrating high accuracy. Moderate overestimation is observed for specimens LE25-Ma and LE32-M, where the STM exceeds the measured capacities by approximately 4–8%; however, these discrepancies remain within acceptable limits for analytical prediction models. The good agreement between STM predictions and experimental results indicates that the anchorage behavior of headed bars can be effectively idealized as a truss mechanism.

Table 7. Comparison of pullout capacity of headed bar (Test and STM)

Model	P_STM (kN)	P_Exp (kN)	P_STM / P_Exp
LE25-M	203.6	203.8	1.000
LE25-Ma	163.9	152.8	1.072
LE19-M	159.0	162.2	0.980
LE32-M	236.7	219.8	1.077
LE25-S	191.8	192.7	0.995
LE25-L	220.5	228.7	0.964

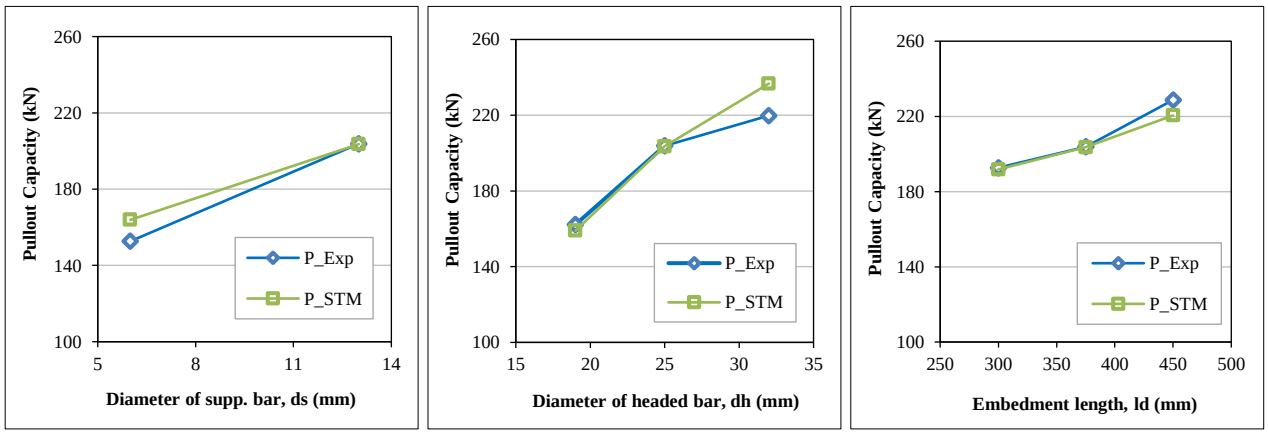

Figure 22. Comparison of pullout capacity of headed bar (Test and STM)

4.3. Parametric Study on STM

Figures 23-a and 23-b compare the experimental pullout capacities with predictions from FEA and STM for different supplementary bar diameters and numbers, respectively. The variation in the supplementary bar was designed to systematically evaluate its role in confinement and strut development. The selected configurations (diameter and number of bars) were chosen to represent realistic detailing options while also enabling isolation of their influence on anchorage performance.

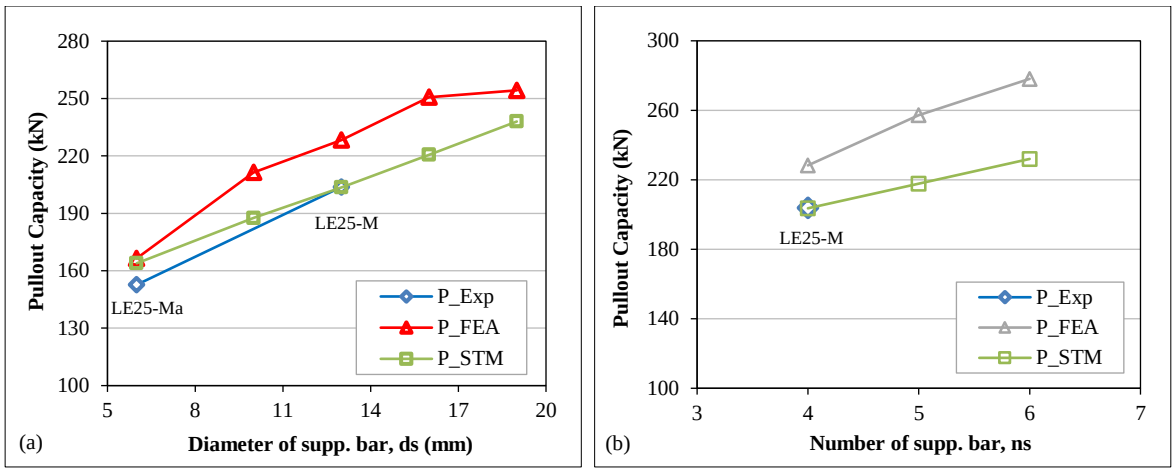

Figure 23. Comparison of parametric study results between FEA and STM

The pullout capacity increases with increasing supplementary bar diameter for all analytical methods, confirming the strong influence of bar diameter on anchorage performance. The STM shows the closest agreement with the experimental results, particularly for intermediate diameters (6–13 mm). In contrast, the FE model consistently predicts higher pullout capacities, indicating an overestimation compared with both the experimental data and the STM results. A similar trend is observed in the number of supplementary bars. The pullout capacity increases as the number of supplementary bars increases, demonstrating the beneficial effect of additional reinforcement on the load-transfer mechanism of the anchorage system. Although the increase predicted by the STM is smaller than that obtained from the FE analysis, the STM captures the overall trend associated with changes in the supplementary reinforcement ratio.

Increasing the diameter of the supplementary bars enlarges the cross-sectional area of the compression strut, thereby increasing its limiting compressive capacity. In addition, adding supplementary bars leads to the formation of additional diagonal compression struts, thereby increasing the pullout load required to reach the strut's limiting compressive capacity. The sensitivity of the STM results to the supplementary bar ratio further confirms that these bars directly influence the geometry and capacity of the compression struts. This provides a clear physical interpretation of the supplementary bar, bridging the gap between empirical observations and analytical modeling.

5. Consideration of Anchorage Capacity Formula

Given that the STM provides the best agreement with the test results and a rational interpretation of the load-transfer mechanism, practical design requires a simplified predictive equation. Therefore, the insights obtained from the STM are translated into a modified empirical formulation.

5.1. Existing Formula of Anchorage Capacity

The anchorage capacity of the specimens was calculated using the empirical formula proposed by Kubota and Murakami, modified by Mohsuni & Matsui [19] (Equation 9), for concrete side blowout failure. The former formula is based on an experimental study of headed bars embedded in T-shaped beam-column joints at middle floors:

$$P_m = k.A_s.\sigma_{std} = k_1.k_2.k_3.k_4.\sigma_{std}.A_s \quad (9)$$

where P_m is the anchorage capacity (kN), A_s is the cross-sectional area of the reinforcing bar (mm^2), and σ_{std} is the stress of the reinforcing bar at anchorage failure (N/mm^2). The relationship between these terms is expressed by the following formula:

$$\sigma_{std} = 101\sqrt{\sigma_B} \quad (10)$$

In the subsequent formula, σ_B represents the compression strength of concrete (N/mm^2). The coefficient k, which influences the anchorage capacity, is then described as follows:

$$k = k_1.k_2.k_3.k_4 \quad (11)$$

k_1 is the influence coefficient of the bearing pressure area ratio (bearing pressure area/cross-sectional area of reinforcing bar) of the anchor plate; $k_1 = 1$, k_2 is the influence coefficient on the cover thickness of concrete, which is expressed as:

$$k_2 = 0.96 + 0.01.\left(\frac{c}{d_h}\right) \quad (12)$$

C is the cover thickness, which is the distance between the side face of the column and the center of the reinforcing bar (mm), d_h is the diameter of the reinforcing bar (mm), k_3 is the influence coefficient of the joint reinforcement bar, which is expressed as:

$$k_3 = 62.5\,\rho_{wj} - 1.22\rho_{wj}(\sigma_B - 27.2) + 1 \geq 1.0 \qquad \text{if } \rho_{wj} \leq 0.4\% \tag{13-a}$$

and

$$k_3 = 1.25\ - 0.0051(\sigma_B - 27.2) \geq 1.0 \qquad \text{if } \rho_{wj} > 0.4\% \tag{13-b}$$

ρ_{wj} is the ratio of supplementary reinforcement bar parallel to the direction of pullout load, where ρ_{wj} = 0%, as supplementary bars parallel to the direction of pullout load are not considered in the cone area. k_4 is the influence coefficient on embedment length (l_d) and the bar diameter (d_b) proposed by Mohsuni & Matsui [19], as follows:

$$k_4 = 0.05\ \frac{l_d}{d_b} - 0.03 \tag{14}$$

5.2. Proposed a New Coefficient for Existing Formula

To validate the influence of the supplementary bar ratio, a more extensive parametric study based on STM was conducted on other specimens (LE25-S, LE25-L, LE19-M, and LE32-M). While only six specimens were tested, they were specifically designed to capture the key parameters governing anchorage behavior and were used to validate the FE and STM models. The results of the parametric study for each model are summarized in Table 8, including LE25-M, which was discussed previously. A total of 35 models were analysed, providing a broader basis beyond the experimental dataset.

Table 8. Parametric study for LE25-M, LE25-S, LE25-L, LE19-M, and LE32-M

n-d_s (mm)	Ratio of supp. bar (%)	LE25-M		LE25-S		LE25-L		LE19-M		LE32-M	
		Pm	P_STM	Pm	P_STM	Pm	P_STM	Pm	P_STM	Pm	P_STM
4-D6	0.091 – 0.144		163.9		157.1		180.5		126.6		197.3
4-D10	0.252 – 0.401		187.6		176.5		202.9		144.8		219.5
4-D13	0.401 – 0.678		203.6		191.8		220.5		159.0		236.7
4-D16	0.645 – 1.027	203.0	220.6	160.5	207.7	246.8	238.8	151.0	174.0	253.5	254.6
4-D19	0.909 – 1.275		238.0		224.2		257.7		189.6		273.3
5-D13	0.532 – 0.847		217.8		201.7		245.5		181.7		245.0
6-D13	0.638 – 1.017		232.0		213.1		252.0		193.5		261.7

Figure 24 presents a comparison between the anchorage capacity predicted by the STM (P_STM) and the calculated capacity (P_m) obtained using the modified Kubota and Murakami formula (Equation 9). Overall, a good agreement is observed, with an average ratio of P_{STM}/P_m = 1.05, indicating that the existing formulation provides a reasonable estimation of anchorage capacity. However, it is important to note that the calculated capacity (P_m) remains constant across all specimen groups, regardless of variations in the supplementary bar ratio (ρ_s). This highlights a key limitation of the existing formulation: its inability to capture the influence of the supplementary bar on anchorage performance

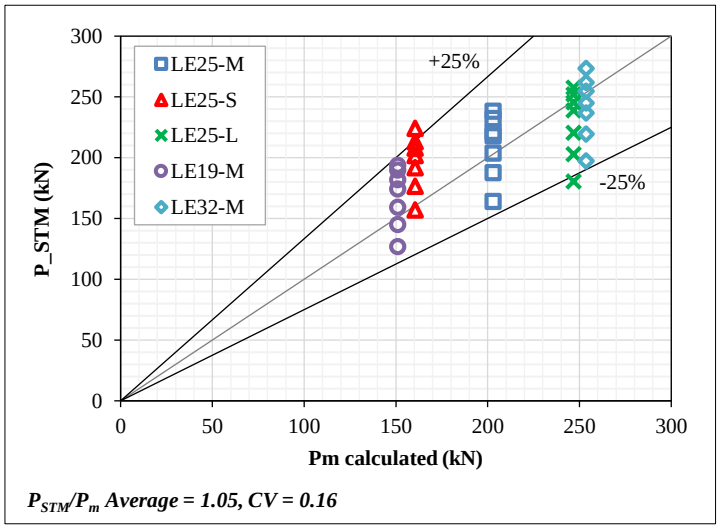

Figure 24. Comparison of P_{STM} and P_m calculated

To address this limitation, Figure 25 examines the relationship between the normalized capacity ratio (P_STM/P_m) and the supplementary bar ratio (ρ_s). A clear trend is observed: the P_STM/P_m increases with increasing supplementary bar ratio. Based on this relationship, a least-squares linear regression analysis is performed, resulting in the introduction of a new coefficient, k_5, defined as a function of ρ_s (Equation 15). This coefficient explicitly accounts for the contribution of the supplementary bar in the analytical formulation.

$$k_5 = 0.38\,\rho_s + 0.81 \tag{15}$$

The new coefficient was added to the original formula, and the proposed modified formula of Kubota and Murakami, based on this study, is as follows:

$$P_{m\_mod} = k_1.k_2.k_3.k_4.k_5.\sigma_{std}.A_s \tag{16}$$

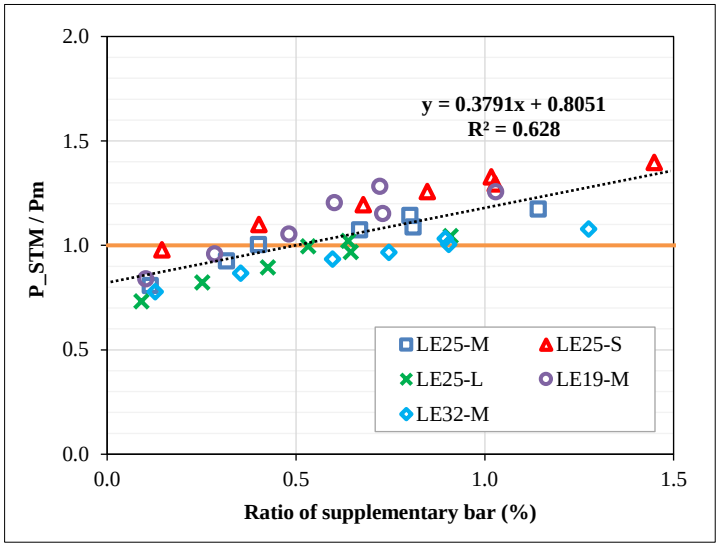

Figure 25. Relationship of anchorage capacities and ratio of supplementary bars

Building on this modification, the anchorage capacity of the specimens was calculated using the modified formula of Kubota and Murakami, and the results are shown in Figure 26. The introduction of the coefficient k_5 provides a quantitative representation of the supplementary bar's influence on anchorage capacity. The observed linear relationship between the supplementary bar ratio and the normalized capacity indicates that the effect of these bars can be systematically incorporated into design formulations. This modification not only improves prediction accuracy but also aligns the empirical model with the underlying physical mechanism, namely the enhancement of compression strut capacity and confinement. To evaluate the accuracy of the proposed approach, various statistical parameters, including mean of P_STM/P_m, standard deviation (SD), and coefficient of variation (CV), are computed. The modifications of the Kubota and Murakami formula yield mean = 1.00, SD = 0.137, and CV = 9.5%, highlighting its reasonable reliability.

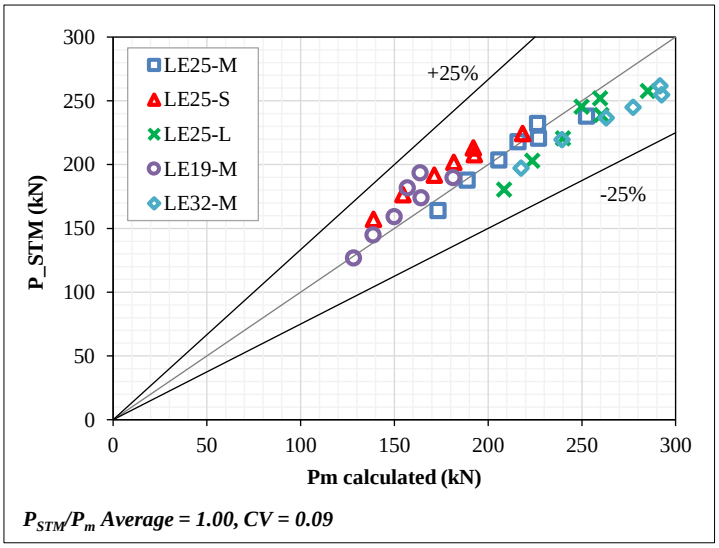

Figure 26. Anchorage capacities based on STM and Modified Kubota and Murakami formula after modification

5.3. Comparison with the Previous Study

To assess the validity and significance of this study, results are compared with prior empirical studies on the anchorage capacity of headed reinforcement bars (Equation 9). The proposed modification to the modified Kubota and Murakami formulation, Equation 16 (with k_5), is evaluated against Equation 9 (without k_5), as shown in Figure 27. The predicted LE25-Ma from Equation 16 indicates that coefficient k_5 provides a quantitative representation of the supplementary bar's influence on anchorage capacity, with a 13% difference from the test results, whereas without it, the difference is 33%. Using the coefficient k_5 improves agreement between calculated and tested capacities. The other specimens also observed a maximum deviation of 19% from the test results, namely in the LE32-M specimen. These findings show that the modification enhances prediction accuracy, reduces statistical dispersion, and provides more reliable estimates of anchorage capacity across various supplementary bar configurations.

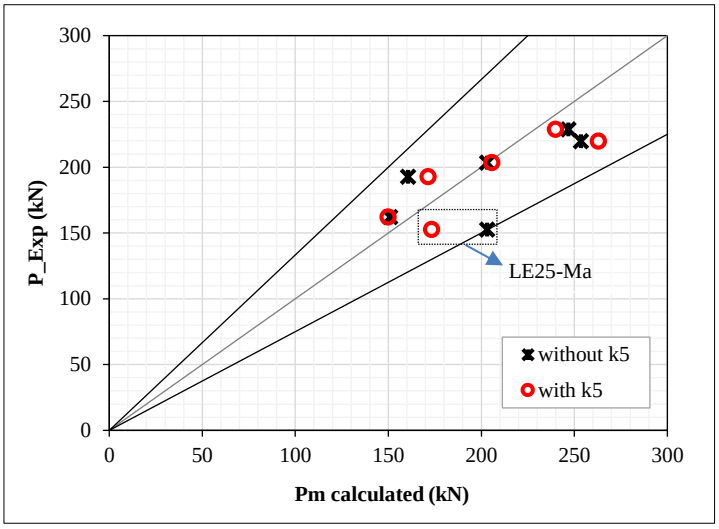

Figure 27. Anchorage capacities based on test and Modified Kubota and Murakami formula before and after modification

6. Conclusions

This study was driven by the need to clarify the role of supplementary bars in the anchorage behavior of headed bars in roof exterior beam–column joints, a condition where confinement is limited and failure is critical. By integrating experimental validation, numerical simulation, and analytical modeling, the study established a consistent understanding of the underlying load-transfer mechanism and translated this understanding into a practical design formulation. The following conclusions can be drawn:

- The non-linear FE model presented in this study accurately predicted the concrete breakout strength of the headed reinforcement bar for experimentally tested roof exterior BCJ specimens. Pullout load-displacement relationships, crack patterns, and reinforcement bar strain results were accurately simulated using FINAL software for the studied specimens.
- The anchorage capacity of the headed bars was substantially impacted by supplementary bars, as indicated by the test and FEA results. The supplementary bars contributed to the concrete's diagonal force to withstand the applied pullout load.
- An STM was developed to predict the pullout capacity of headed reinforcement bars governed by concrete cone failure. The model geometry was derived from stress distributions obtained through FEA and experimental observations, with the primary compressive strut identified as the governing failure component. An optimization procedure was used to determine the strut forces and cross-sectional area, leading to a simple expression for the effective strut width.
- The proposed STM shows very good agreement with experimental results for all tested specimens, with predicted-to-measured capacity ratios ranging from 0.98 to 1.11 and differences within 2% for most cases.
- Parametric studies demonstrate that increasing the diameter and number of supplementary bars significantly enhances pullout capacity. Models with larger-diameter or more supplementary bars demonstrated noticeably higher breakout.
- By introducing a new coefficient derived from regression analysis of STM results, the modified Kubota and Murakami formulation achieved improved predictive accuracy and reduced statistical dispersion. The proposed coefficient can be used as a new effectiveness factor in predicting the anchorage performance of headed bars influenced by supplementary bars.

Implications: The parametric study confirms that increasing the supplementary bar ratio significantly enhances the anchorage capacity of headed bar. This improvement is attributed to the enlargement of the effective compression strut area and improved confinement within the joint core. These results emphasize that supplementary reinforcement bars should not be treated merely as secondary detailing, but rather as active structural components in anchorage design. Although the study focuses on roof exterior BCJs, the fundamental load-transfer mechanisms identified (namely the formation of diagonal compression struts and the confinement effect of supplementary bar) are not unique to this joint type. These mechanisms are governed by local stress conditions around the headed bar and are expected to be applicable to other BCJ types, including interior joints.

Limitations and Future Work: In the present study, the specimen configuration included only two-headed bars to investigate the strut mechanism associated with the concrete breakout strength developed by the headed and supplementary reinforcement. However, in practical structural applications, the primary reinforcement typically consists of more than two bars. Therefore, future research should include experimental investigations on specimens incorporating three and four-headed bars to better represent actual structural conditions.

7. Declarations

7.1. Author Contributions

Conceptualization, Z.A.J. and T.M.; methodology, Z.A.J.; software, T.M.; validation, Z.A.J. and T.M.; formal analysis, Z.A.J.; investigation, Z.A.J.; resources, T.M.; data curation, T.M.; writing—original draft preparation, Z.A.J. and T.M.; writing—review and editing, Z.A.J. and T.M.; visualization, Z.A.J.; supervision, T.M.; funding acquisition, T.M. All authors have read and agreed to the published version of the manuscript.

7.2. Data Availability Statement

The data presented in this study are available on request from the corresponding author.

7.3. Funding

The authors received no financial support for the research, authorship, and/or publication of this article.

7.4. Conflicts of Interest

The authors declare no conflict of interest.

8. References

[1] Ghimire, K. P., Shao, Y., Darwin, D., & O'Reilly, M. (2019). Conventional and high-strength headed bars-Part 1: Anchorage tests. ACI Structural Journal, 116(3), 255–264. doi:10.14359/51714479.

[2] ACI 318-02. (2002). Building Code Requirements for Structural Concrete and Commentary. American Concrete Institute (ACI), Farmington Hills, United States.

[3] Miao, T., Yang, J., Zhou, Y., Zhan, M., Sha, L., & Zheng, W. (2023). Research on the Distributive Relationship between Bond Force and Bearing Pressure for Anchorage Force by Headed Bars. Buildings, 13(10), 2463. doi:10.3390/buildings13102463.

[4] Hasselwander, G. B., Jirsa, J. O., Breen, J. E., & Lo, K. (1977). Strength and Behavior of Anchor Bolts Embedded Near Edges of Concrete Piers. Research Project 3-5-74-29. NASA STI/Recon Technical Report N, 78, 29278, National Aeronautics and Space Administration (NASA), Washington, United States.

[5] Wallace, J. W., McConnell, S. W., Gupta, P., & Cote, P. A. (1998). Use of headed reinforcement in beam-column joints subjected to earthquake loads. ACI Structural Journal, 95(5), 590–606. doi:10.14359/574.

[6] Wright, J. L., & McCabe, S. L. (1997). The development length and anchorage behavior of headed reinforcing bars. University of Kansas Center for Research, Lawrence, United States.

[7] DeVries, R. A. (1996). Anchorage of headed reinforcement in concrete. Ph.D. thesis, University of Texas at Austin, Austin, United States.

[8] de Barros Santos, J. P., de Oliveira, M. H., Lima, N. W. B., Pereira Filho, M. J. M., & de Pina Ferreira, M. (2024). A parametric finite element study of concrete cone failure in headed bars under tensile loading. Latin American Journal of Solids and Structures, 21(2), 2. doi:10.1590/1679-78257940.

[9] Xu, Y., Chen, C., Xie, M., & Gong, J. (2024). Experimental Study of the Influence of Supplementary Reinforcement on Tensile Breakout Capacity of Headed Anchors in Nuclear Power Plant Equipment Foundations. Buildings, 14(9), 1–17. doi:10.3390/buildings14093027.

[10] Thompson, M. K. (2002). The anchorage behavior of headed reinforcement in CCT nodes and lap splices. Ph.D. Thesis, The University of Texas at Austin, Austin, United States.

[11] Thompson, M. K., Jirsa, J. O., & Breen, J. E. (2006). CCT nodes anchored by headed bars - Part 2: Capacity of nodes. ACI Structural Journal, 103(1), 65–73. doi:10.14359/15087.

[12] Ananda, R., & Imran, I. (2017). Force Transfer Mechanism of Headed Anchorage Bar in Exterior Beam Column Joint with Finite Element Method and Strut and Tie Model. IPTEK Journal of Proceedings Series, 3(6), 307–317. doi:10.12962/j23546026.y2017i6.3266.

[13] Yuan, L., Yang, Y., Wang, Q., Zhao, Q., Cui, Y., & Zhao, W. (2025). Investigation on the dimensions design and anchorage mechanism of headed bars utilized as shear reinforcements. Structures, 75, 108647. doi:10.1016/j.istruc.2025.108647.

[14] Mirzagulpour, A., Yousefpour, H., & Mozafari, A. (2026). Anchorage performance of headed bars in concrete affected by alkali silica reaction. Engineering Structures, 354, 122413. doi:10.1016/j.engstruct.2026.122413.

[15] Eswar, M., & Chourasia, A. (2026). Numerical study on the performance of SMA-reinforced beam-column joints with headed bar connections. Structures, 85, 111133. doi:10.1016/j.istruc.2026.111133.

[16] Abdelwahed, B. S. (2026). Analytical and modeling studies on discontinuity regions in reinforced concrete elements: review article. Innovative Infrastructure Solutions, 11(4), 207. doi:10.1007/s41062-026-02537-w.

[17] Isikli, Y., Binici, B., Arici, Y., & Tuncay, K. (2026). Strut and tie models with the dual use of the finite element method and the lattice networks. Engineering Structures, 346, 121661. doi:10.1016/j.engstruct.2025.121661.

[18] Mohsuni, H., Matsui, T., Sanada, Y., Sakuta, J., Kiyohara, T., Kim, Y., & Adachi, T. (2023). Pullout Tests on Concrete Breakout Strength of Headed Reinforcement Bars Embedded in Roof Exterior Beam-Column Joints. Journal of Advanced Concrete Technology, 21(5), 392–404. doi:10.3151/jact.21.392.

[19] Mohsuni, H., Matsui, T. (2023). Experimental Study of Concrete Breakout Strength for Headed Reinforcement Bars Embedded in Roof Exterior Beam-Column Joints. Building for the Future: Durable, Sustainable, Resilient. *fib* Symposium 2023, Lecture Notes in Civil Engineering, Springer, Cham, Switzerland. doi:10.1007/978-3-031-32511-3_20.

[20] Murakami, M., Fuji, T., & Kubota, T. (1997). Evaluation of Mechanical Anchorage Capacities of Main Bars in Beam-column Joints Based on Pull-out Tests. Concrete Research and Technology, 8(2), 1–10. doi:10.3151/crt1990.8.2_1.

[21] CTC (2018). ITOCHU Techno-Solutions Corporation. CTC, Minato, Japan Available online: https://www.ctc-g.co.jp/en/company/release/?year=2018 (accessed on April 2026).

[22] Naganuma, K. (1995). Stress-Strain Relationship for Concrete Under Triaxial Compression. Journal of Structural and Construction Engineering (Transactions of AIJ), 60(474), 163–170. doi:10.3130/aijs.60.163_2.

[23] Nakamura, H. (1999). Compressive fracture energy and fracture zone length of concrete. JCI-C51E Post-Peak Behavior of RC Structures subjected to Seismic Loads, 2, 259-272.

[24] Izumo, J., Shima, H., & Okamura, H. (1987). Analytical Model for Reinforced Concrete Panel Elements Subjected to In-Plane Forces. Concrete Journal, 87.9-1, 107–120. doi:10.3151/coj1975.25.9_107. (In Japanese).

[25] Naganuma, K. (1991). Nonlinear Analytical Model for Reinforced Concrete Panels Under In-Plane Stresses: Study on nonlinear analytical method for reinforced concrete wall structures (Part 1). Journal of Structural and Construction Engineering (Transactions of AIJ), 421(0), 39–48. doi:10.3130/aijsx.421.0_39. (In Japanese).

[26] Vecchio, F. J., & Collins, M. P. (1986). Modified Compression-Field Theory for Reinforced Concrete Elements Subjected to Shear. Journal of the American Concrete Institute, 83(2), 219–231. doi:10.14359/10416.

[27] Naganuma, K., Yonezawa, K., Kurimoto, O., & Eto, H. (2004). Simulation of nonlinear dynamic response of reinforced concrete scaled model using three-dimensional finite element method. 13th World Conference on Earthquake Engineering, 1-6 August, 2004, Vancouver, Canada.

[28] Walraven, J. (2013). fib Model Code for Concrete Structures 2010: mastering challenges and encountering new ones. Structural Concrete, 14(1), 3-9. doi:10.1002/suco.201200062.

[29] ACI 318-19. (2019). Building Code Requirements for Structural Concrete and Commentary. American Concrete Institute (ACI), Farmington Hills, United States. doi:10.14359/51716937.

[30] Halim, S., Takahashi, S., Ichinose, T., Teshigawara, M., Kamiya, T., & Fukuyama, H. (2014). Strength of beam-column joint in soft first story of RC buildings Part 2: Design equations. Journal of Advanced Concrete Technology, 12(5), 146–157. doi:10.3151/jact.12.146.

[31] AASHTO LRFD. (1998). Bridge Design Specifications. American Association of State Highway and Transportation Officials (AASHTO), Washington, United States.

[32] Yun, Y. M., & Ramirez, J. A. (1996). Strength of Struts and Nodes in Strut-Tie Model. Journal of Structural Engineering, 122(1), 20–29. doi:10.1061/(asce)0733-9445(1996)122:1(20).

[33] CAN3-A23.3-M94. (1994). Code for the design of concrete structures for buildings. Canadian Standards Association (CSA), Toronto, Canada.

[34] Canadian Ministry of Transportation. (1991). Ontario Highway Bridge Design Code (3rd Ed.). Canadian Ministry of Transportation, Toronto, Canada.